Biosensors and Bioelectronics 77 (2016) 557–564

Contents lists available at ScienceDirect

Biosensors and Bioelectronics

journal homepage: www.elsevier.com/locate/bios

CdS/MoS_2 heterojunction-based photoelectrochemical DNA biosensor via enhanced chemiluminescence excitation

Yang Zang, Jianping Lei *, Qing Hao, Huangxian Ju

State Key Laboratory of Analytical Chemistry for Life Science, Collaborative Innovation Center of Chemistry for Life Sciences, School of Chemistry and Chemical Engineering, Nanjing University, Nanjing 210093, PR China

ARTICLE INFO

Article history:
Received 9 August 2015
Received in revised form
1 October 2015
Accepted 4 October 2015
Available online 8 October 2015

Keywords:
Photoelectrochemistry
Biosensors
Quantum dots
MoS_2
DNA detection

ABSTRACT

This work developed a CdS/MoS_2 heterojunction-based photoelectrochemical biosensor for sensitive detection of DNA under the enhanced chemiluminescence excitation of luminol catalyzed by hemin–DNA complex. The CdS/MoS_2 photocathode was prepared by the stepwise assembly of MoS_2 and CdS quantum dots (QDs) on indium tin oxide (ITO), and achieved about 280% increasing of photocurrent compared to pure CdS QDs electrode due to the formation of heterostructure. High photoconversion efficiency in the photoelectrochemical system was identified to be the rapid spatial charge separation of electron–hole pairs by the extension of electron transport time and electron lifetime. In the presence of target DNA, the catalytic hairpin assembly was triggered, and simultaneously the dual hemin-labeled DNA probe was introduced to capture DNA/CdS/MoS_2 modified ITO electrode. Thus the chemiluminescence emission of luminol was enhanced via hemin-induced mimetic catalysis, leading to the physical light-free photoelectrochemical strategy. Under optimized conditions, the resulting photoelectrode was proportional to the logarithm of target DNA concentration in the range from 1 fM to 100 pM with a detection limit of 0.39 fM. Moreover, the cascade amplification biosensor demonstrated high selectivity, desirable stability and good reproducibility, showing great prospect in molecular diagnosis and bioanalysis.

1. Introduction

Photoelectrochemical DNA bioassays have attracted widespread attention in analytical community owing to its low background signal and excellent sensitivity (Haddache et al., 2014; Zhao et al., 2014). The considerable efforts have been developed to design photoelectrochemical platform based on various nanomaterials such as metal oxide (Lu et al., 2006; Wu et al., 2013), two-dimensional nanosheets (Zhuang et al., 2015), metal nanoparticles (Li et al., 2014; Lu et al., 2008), quantum dots (QDs) (Long et al., 2011) and their nanohybrids (Zhang et al., 2012). Among them, CdS QDs with a narrow gap band of ~2.4 eV has emerged as an attractive photoactive material (Gill et al., 2008; Sun et al., 2008; Xiao et al., 2014), showing a visible light-driven photoelectricity activity. However, pure CdS QDs suffers from the rapid recombination of photogenerated electron–hole pairs (Zhang et al., 2015; Zhao et al., 2015), which limits its incident photon to current conversion efficiency. To alleviate this restriction, two different semiconductors with matched energy levels can be employed to enhance the charge transfer rate, resulting in the improved photoelectrochemical performance.

Semiconductor molybdenum disulfide (MoS_2), as a typical transition-metal dichalcogenide composed of S–Mo–S triple layers which are bounded by van der Waals forces, has aroused increasing academic interest due to its unique optical, electronic and catalytic properties (Gao et al., 2015; Ou et al., 2014). In particular, MoS_2 nanosheets as cocatalyst can accept electrons to accelerate photocatalytic hydrogen evolution within semiconductor-based devices (Bai et al., 2015; Chen et al., 2015). For instance, MoS_2 nanosheets-coated TiO_2 nanobelt exhibited a desirable photocatalytic hydrogen reaction activity, suggesting the matched energy band of TiO_2@MoS_2 hybrids favor the suppression of photoelectron–hole recombination (Zhou et al., 2013). When ultrathin MoS_2 nanosheets were confined to zero dimensions, the MoS_2 QDs would give rise to the interesting physical properties with abundant exposed catalytic edge sites and excellent intrinsic conductivity of monolayer structure (Gopalakrishnan et al., 2015; Ren et al., 2015). However, studies on MoS_2 QDs-based biosensing have been less reported owing to the lack of surface functional groups. To expanding its application range, CdS nanocrystals can be integrated by layer-by-layer assembly technique to construct the MoS_2 QDs-based heterogeneous structure for developing a versatile photoelectrochemical sensing platform with efficient

* Corresponding author. Tel./fax: +86 25 83593593.
E-mail address: jpl@nju.edu.cn (J. Lei).

http://dx.doi.org/10.1016/j.bios.2015.10.010
0956-5663/

separation of electron–hole pairs.

To further enhance the detection signal, DNA recycling strategies such as catalytic hairpin assembly (CHA) (Qing et al., 2014), hybridization chain reaction (Chen et al., 2012) and rolling circle amplification (Russell et al., 2014) have been employed for DNA bioassays, in which the signal amplification is achieved by allowing a single target DNA to interact with multiple nucleic acid-based signal probes. Among them, owing to the desirable programmability and hundreds-fold signal amplification ability, CHA has been successfully applied in biosensors with fluorophores or redox tags as reporters (Hun et al., 2015; Qian et al., 2015; Song et al., 2015). On the other hand, enzymatic catalysis is also an efficient way to improve the sensitivity. Especially, mimetic catalysts have been extensively investigated as low-cost alternatives of natural enzymes due to the convenient synthesis and high stability (Garai-Ibabe, et al., 2014; Willner et al., 2008; Xu and Dong, 1999). For instance, a facile label-free electrochemiluminescent DNA sensor was designed via target-induced hemin/G-quadruplex switching to catalyze the reduction of dissolved oxygen for signal inhibition (Deng et al., 2013). However, compared to hemin/G-quadruplex, hemin-labeled DNA as an alternative not only remains the high catalytic activity of luminol oxidation in the presence of H_2O_2, but also shows outstanding designability and adaptability to DNA assembly because of its low steric hindrance, which was favorable to design various bioassay methods for highly sensitive detection of trace analyst (Zhang et al., 2011).

In this work, by integrating the advantages of CdS/MoS_2 heterojunction, CHA and hemin-mediated chemiluminescence, we present a novel strategy for photoelectrochemical detection of DNA. As shown in Scheme 1, the capture DNA (C-DNA) was immobilized on CdS/MoS_2 modified ITO electrode surface via the amide reaction. In the presence of target DNA (tDNA), the hairpin structure of C-DNA could be opened, and then the dual hemin-labeled DNA probe (HLDP) can initiate CHA recycling, followed by the formation of HLDP:C-DNA duplex on electrode surface. Subsequently, hemin as a mimic enzyme can in situ catalyze luminol oxidation to generate chemiluminescence (CL). Under CL irradiation, photogenerated CdS QDs can produce electron–hole pairs. With the migration of conduction band (CB) electrons to ITO electrode and the concomitant scavenging of valence band (VB) holes by H_2O_2, the increased photocurrent was obtained due to the spatial separation of charge carriers. Therefore, based on the high photoelectric conversion efficiency of CdS/MoS_2 heterostructure as well as CHA-programmed HLDP:C-DNA duplex as signal probe, the designed biosensor exhibits an excellent performance with desirable selectivity and detection limit down to femtomolar level, showing a promising application in bioanalysis.

2. Experimental section

2.1. Materials and reagents

Indium tin oxide (ITO) electrode was purchased from Zhuhai Kaivo Electronic Components Co. Ltd. (China). Cadmium chloride ($CdCl_2$), thioglycolic acid (TGA), luminol ($\geq$97%), 1-ethyl-3-(3-(dimethylamino)propyl)carbodiimide (EDC), n-hydroxysuccinimide (NHS), molybdenum(IV) sulfide (MoS_2), ascorbic acid (AA) and monoethanolamine (MEA) were purchased from Sigma-Aldrich. $Na_2S \cdot 9H_2O$ was obtained from Shanghai Lingfeng Chemical Reagent Co. Ltd. All other chemicals were of analytical grade without further purification. All aqueous solutions were prepared using ultrapure water obtained from a Millipore water purification system ($\geq$ 18 MΩ, Milli-Q, Millipore). The washing buffer was 10 mM PBS of pH 7.4 containing 300 mM NaCl. The CHA reaction was performed in 20 mM Tris–HCl of pH 7.4 containing 100 mM NaCl and 5 mM $MgCl_2$. All the oligonucleotides were synthesized and purified by TAKARA Biotechnology (Dalian, China) and their sequences are listed as follows:

Target DNA: 5′-GTGTCGTCTTCAGAATACCATGCT-3′

Capture DNA: 5′-NH_2-TTTTTTAGCATGGTATTCTGAAGACGACAC TACCATGCTT GATCGTCT TCAGAATAC-3′

Hairpin DNA (H-DNA): 5′-GTTATTAATGTGTGATGTTGAA-GACGATCAAGCATGG TAGTGTCGTCTTCAGAATACCATGCTTGATCG-3′

Dual hemin-labeled DNA (2 HP): 5′-hemin-ACATCACACATTAA-TAAC-hemin-3′

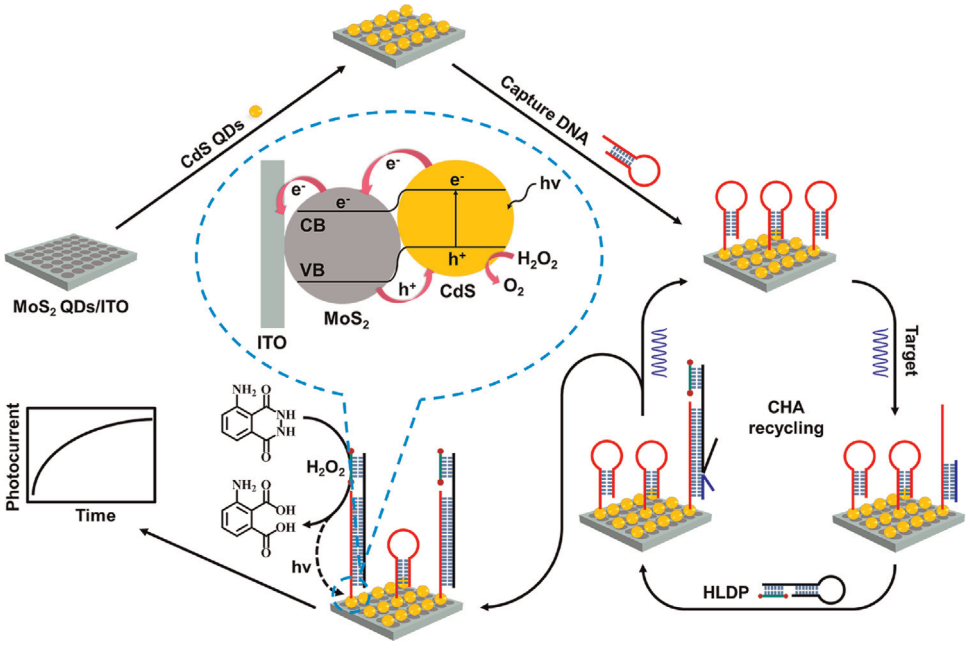

Scheme 1. Schematic illustration for CdS/MoS_2 heterojunction-enhanced photoelectrochemical sensing strategy coupling with CHA and hemin-mediated chemiluminescence.

Label-free DNA probe: 5′-ACATCACACATTAATAAC-3′

Single-base mismatched DNA (smDNA): 5′-GTGTCGTCTTCA-CAATACCAT GCT-3′

Three-base mismatched DNA (tmDNA): 5′-GTGTCATCTTCA-CAATACGATG CT-3′

2.2. Apparatus

Transmission electron micrographs (TEM) were performed using a JEM-2100 microscope (JEOL, Japan). Fluorescence (FL) measurements were conducted on a RF-5301PC fluorescence spectrometer (Shimadzu Co. Japan) equipped with a xenon lamp. UV–vis absorption spectra were obtained using a UV-3600 UV–vis–NIR spectrophotometer (Shimadzu Co. Kyoto, Japan). The CL spectrum was recorded on an IFFM-E Luminescent Analyzer (Remax, China). Photoelectrochemical measurements without excitation light were carried out with a home-built photoelectrochemical system. Other photocurrent–time, intensity-modulated photocurrent spectroscopy (IMPS) and intensity-modulated photovoltage spectroscopy (IMVS) measurements were detected on a Zahner intensity modulated photospectrometer (Zahner, German) with a LW430 light as the accessory excitation source. Current–voltage (*I–V*) experiments were performed on a CHI 660D electrochemical workstation (CH Instruments Inc., USA). Electrochemical impedance spectroscopy (EIS) was conducted using a PGSTAT30/FRA2 system (Autolab, The Netherlands) in 0.1 M Na_2SO_4 solution containing 5 mM $K_4[Fe(CN)_6]/K_3[Fe(CN)_6]$ (1:1) mixture as the redox probe from 0.1 Hz to 100 kHz with a signal amplitude of 5 mV and the applied potential of 0.180 V. All experiments were performed at room temperature using a conventional three-electrode system with a modified ITO electrode as the working, platinum electrode as the auxiliary, and saturated calomel as the reference electrodes.

2.3. Preparation of MoS_2 QDs

MoS_2 QDs was obtained by liquid exfoliation according to the reported method with slight modifications (Zhou et al., 2011). Typically, 600 mg of MoS_2 powder was added into 200 ml of ethanol/water with ethanol volume fraction of 45%, and then ultrasonicated for 24 h. The initially formed suspension was thrice centrifuged at 6000 rpm for 20 min, and filtered through 0.22 μm ultrafiltration membranes to remove the residual unexfoliated aggregates. Then the supernatant was collected and concentrated on a rotary evaporator at 60 °C under reduced pressure. The resulting precipitate was resuspended in deionized water and filtered through 0.22 μm ultrafiltration membranes again. Finally, the prepared MoS_2 QDs was kept at 4 °C before usage.

2.4. Construction of photoelectrochemical biosensor

The TGA-capped CdS QDs was synthesized using a previously reported recipe (Zang et al., 2015). Prior to the fabrication of designed biosensor, the ITO electrode was immersed in boiling 2-propanol solution containing 1.0 M NaOH for 15 min, followed by ultrasonic cleaning with 10% H_2O_2, acetone and deionized water. The CdS/MoS_2 modified ITO electrode was prepared as follows: first, 10 μL of MoS_2 QDs was applied to the ITO electrode and dried at room temperature. Sequentially, 10 μL of CdS QDs was dropped onto the electrode to obtain CdS/MoS_2 heterogeneous structure via a non-covalent interaction. The carboxylic group of QDs was activated using 10 mM PBS buffer of pH 5.3 containing 10 mM EDC and 20 mM NHS for 1 h at room temperature. After the activated electrode was rinsed with PBS buffer, 20 μL of 1.0 μM C-DNA was dropped onto electrode surface and incubated at 4 °C overnight. Then the electrode was rinsed three times to remove the non-conjugated DNA. Finally, the modified electrode was blocked with 20 μL of 1 mM MEA for 2 h at 4 °C and rinsed with washing buffer thoroughly.

2.5. Photoelectrochemical detection of DNA

Similar to the preparation of C-DNA, H-DNA was annealed at 90 °C for 5 min followed by slowly decreasing to room temperature. Then H-DNA and 2HP (1:1 of molar ratio) were incubated for 1 h to form HLDP prior to photoelectrochemical experiments. After mixing with target DNA, the CHA reaction was triggered at room temperature for 2.5 h. Finally, the modified electrode was rinsed with PBS buffer, and the photoelectrochemical signal was recorded in 0.1 M Tris–HCl buffer of pH 9.0 containing 20 mM H_2O_2, and 1.0 mM luminol at a constant potential of +0.2 V for DNA detection without deaeration.

3. Results and discussion

3.1. Characterization of MoS_2 QDs

Liquid exfoliation technique is a powerful way to break the weak interlayer forces in bulk materials to get small nanoparticles by simple sonication. Considering the broad application of MoS_2 nanomaterial in field effect transistor (Choi et al., 2015; Singh et al., 2014), photocatalysis (Kang et al., 2015) and bioanalysis (Wang et al., 2014), here, a highly dispersed suspension of MoS_2 QDs was prepared by liquid exfoliation method. Compared to bulk MoS_2 (Fig. 1A), the TEM image of MoS_2 QDs clearly showed round-shaped morphology with an average size of 3.5 nm (Fig. 1B).

In order to characterize the structural properties of MoS_2 QDs, UV–vis absorption spectrum was recorded for as-prepared sample (Fig. 1C). The weaker threshold at 390 nm could be assigned to the direct transition from the deep valence band to the conduction band (Gopalakrishnan et al., 2014), while the absorption peaks below 300 nm was assigned to the excitonic feature of MoS_2 QDs (Chikan and Kelley, 2002). In addition, the FL spectrum of MoS_2 QDs was measured under 290 nm excitation wavelength (Fig. 1D). A typical FL emission peak was observed at ca. 419 nm, which was identical with the result reported in literature (Ha et al., 2014), confirming the successful preparation of MoS_2 QDs.

3.2. Feasibility of photoelectrochemical strategy

Fig. 2A displayed UV–vis spectra of different structural DNA. Compared to the label-free DNA probe (curve a), dual hemin-labeled DNA showed not only a typical absorption peak of DNA at 260 nm but also a broad absorption peak of hemin at 378 nm (curve b), which was attributed to covalent assembly of DNA and hemin. When the mixture of H-DNA and dual hemin-labeled DNA was incubated for 1 h, a clear red shift from 378 nm to 403 nm was observed as well as an appreciably enhancement of absorption intensity (curve c). This result could be assigned to the existence of active monomers of hemin species benefited from the rigid structure of formed HLDP.

Fig. 2B examined the CL spectrum of HLDP and UV–vis absorption spectrum of CdS QDs. The chemiluminescence, resulted from hemin-catalyzed luminol oxidation using H_2O_2 as an oxidant, had a maximum emission peak at ca. 425 nm (curve a), whereas CdS QDs showed a broad absorption below 500 nm (curve b). Apparently, the CL spectrum of luminol oxidation and the absorption spectrum of CdS QDs were highly overlapped in a wide wavelength range, demonstrating luminol-based chemiluminescence as excitation light could apply to the construction of photoelectrochemical biosensor (Golub et al., 2012).

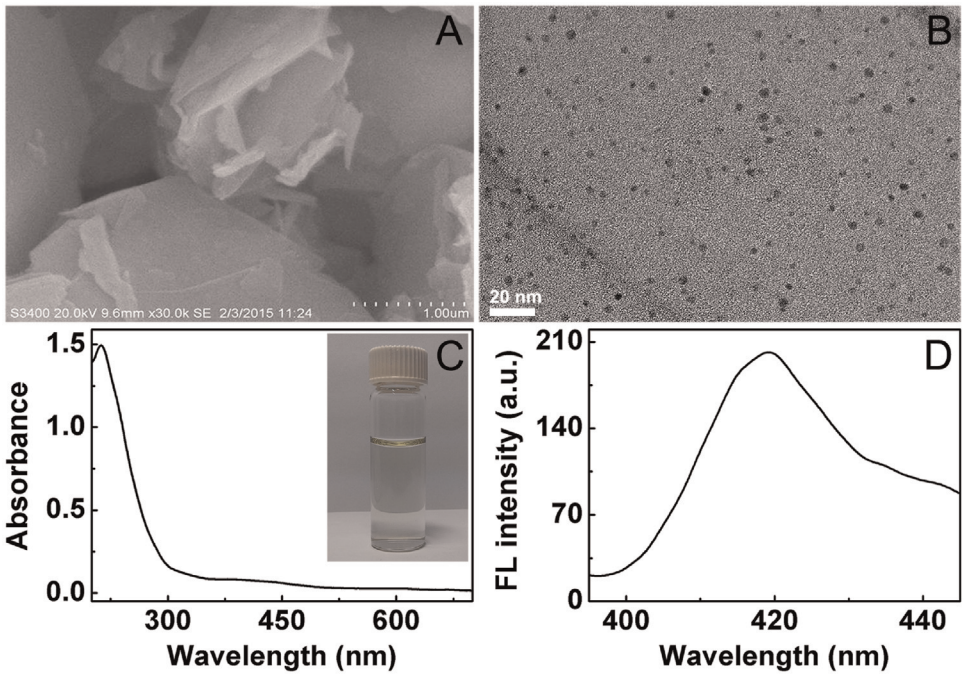

Fig. 1. (A) SEM image of bulk MoS_2, (B) TEM image, (C) UV–vis and (D) FL spectra of MoS_2 QDs. Inset of panel C is the photography of MoS_2 QDs solution.

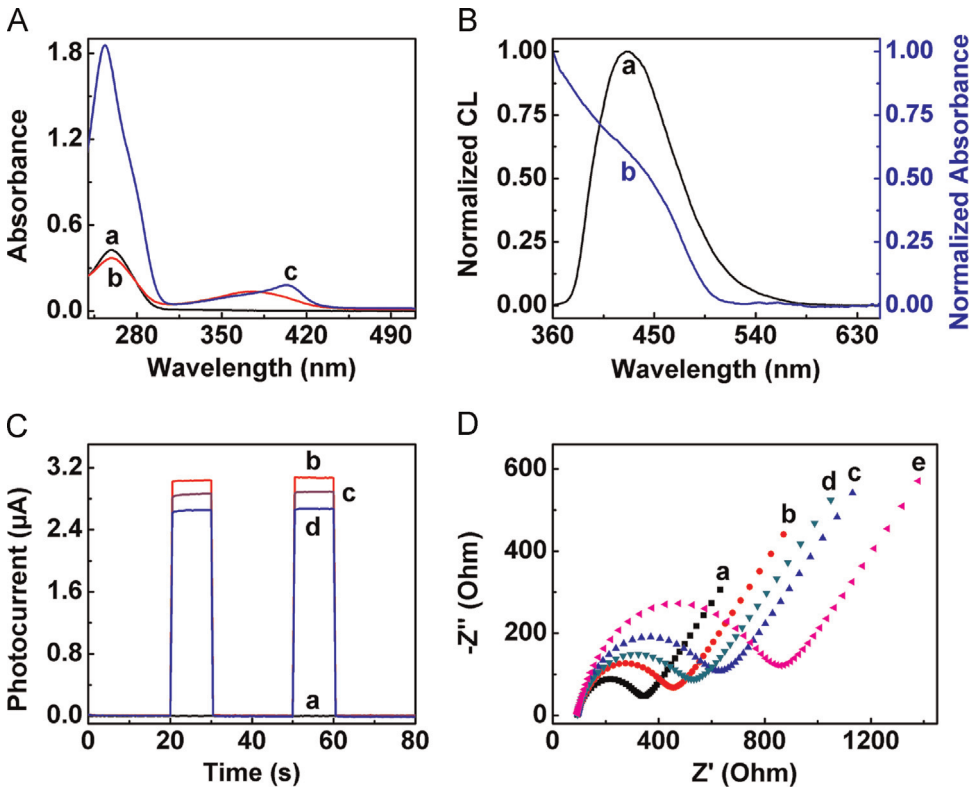

Fig. 2. (A) UV–vis spectra of 2 μM label-free DNA probe (a), dual hemin-labeled DNA (b) and HLDP (c). (B) HLDP-mediated chemiluminescence spectrum of luminol (a) and UV–vis absorption spectrum of CdS QDs (b). (C) Photocurrent responses of MoS_2 (a), CdS/MoS_2 (b), C-DNA/CdS/MoS_2 (c), and HLDP:C-DNA/CdS/MoS_2 (d) modified ITO electrodes in PBS buffer of 7.4 containing 0.1 M AA as electron donor. Excitation light: 430 nm. (B) Impedance spectra of MoS_2 (a), CdS/MoS_2 (b), C-DNA/CdS/MoS_2 (c), (c) blocked by MEA (d), and HLDP:C-DNA/CdS/MoS_2 (e) modified ITO.

To identify the effect of steric hindrance on the photocurrent, AA was employed to use as electron donor in photocurrent–time experiments (Fig. 2C). As shown in curve a, no photocurrent was observed for MoS_2 modified ITO electrode, suggesting MoS_2 QDs was not excited under 430 nm irradiation. After modification of CdS QDs, the photocurrent response significantly increased with the excitation of QDs (curve b). However, when C-DNA and MEA were sequentially applied to the electrode surface (curve c), the

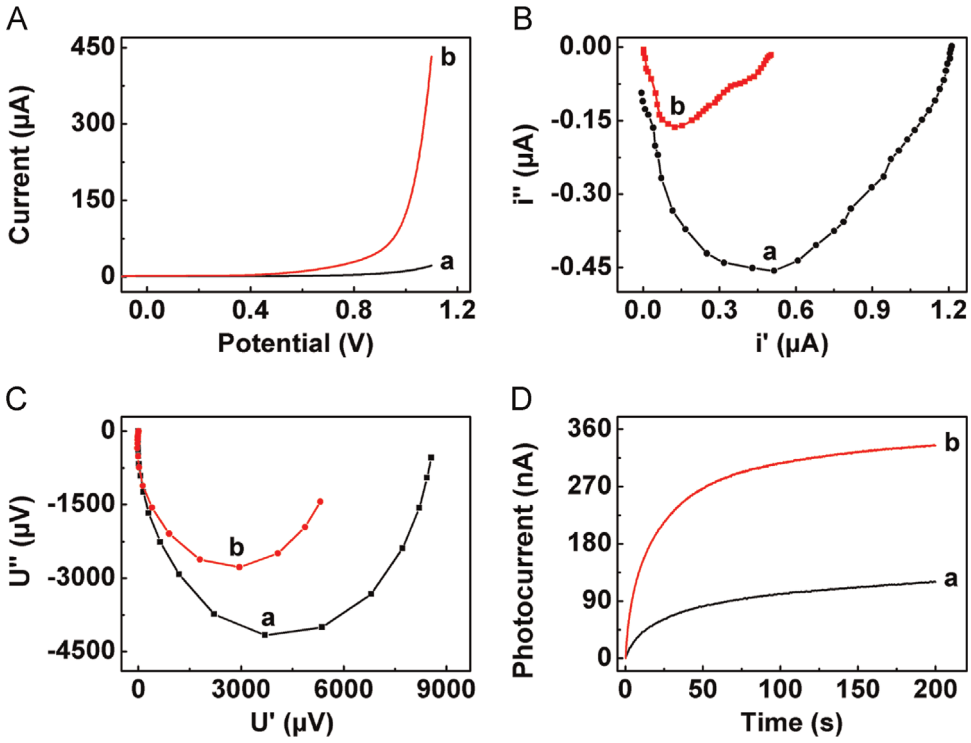

Fig. 3. (A) *I–V* curves, (B) IMPS, and (C) IMVS of CdS (a) and CdS/MoS_2 (b) modified ITO electrodes in Tris–HCl buffer of pH 9.0 containing 1 mM H_2O_2. (D) Photocurrent response of HLDP:C-DNA/CdS (a) and HLDP:C-DNA/CdS/MoS_2 (b) modified ITO electrodes in 0.1 M Tris–HCl buffer of pH 9.0 containing 20 mM H_2O_2 and 1.0 mM luminol.

photocurrent value was declined owing to the effect of steric hindrance. Likewise, after hybridization with target DNA followed by CHA reaction (curve d), more HLDP was immobilized onto C-DNA/CdS/MoS_2 modified ITO electrode, leading to further decrease of photocurrent.

The stepwise fabrication of biosensor was also investigated by EIS (Fig. 2D). For MoS_2 modified ITO electrode, the impedance spectrum showed a small R_{ct} of 237.1 Ω (curve a). When CdS QDs and C-DNA was sequentially immobilized onto MoS_2/ITO electrode, the R_{ct} increased to 342 Ω (curve b) and 506.3 Ω (curve c), suggesting the low conductivity of QDs and the large steric hindrance of DNA. After blocked with MEA, the R_{ct} value declined to 416.2 Ω because of the electrostatic interaction between the positively charged MEA and the negatively charged redox probe (curve d). Moreover, the value of R_{ct} significantly increased to 726.2 Ω after the formation of HLDP:C-DNA duplex resulted from target-initiated CHA reaction (curve e), which was demonstrated that the designed biosensor was feasible as expected.

3.3. Characterization of CdS/MoS_2 heterojunction

I–V experiments were conducted to confirm the heterojunction configuration of CdS/MoS_2 with a potential range of $-0.1 \sim +1.1$ V at a scan rate of 100 mV s^{-1} (Fig. 3A). The prompt increment of anodic current at CdS/MoS_2/ITO electrode (curve b) was observed at potentials higher than 0.8 V compared to that of CdS/ITO electrode (curve a), which can be attributed to the appearance of electrical breakdown, indicating the formation of heterojunction.

In order to better understand photogenerated electron transfer property of CdS/MoS_2, the IMPS and IMVS techniques were measured under 430 nm light with the intensity of 8 mW cm^{-2}. The electron transport time (τ_d) and electron lifetime (τ_n) can be calculated by the expressions $\tau_d = 1/2\pi f_{IMPS}$ and $\tau_n = 1/2\pi f_{IMVS}$, where f_{IMPS} and f_{IMVS} are the frequency of the minimum IMPS and IMVS imaginary components, respectively (Krüger et al., 2003; Wang et al., 2013). As shown in Fig. 3B, the τ_d of CdS/MoS_2/ITO electrode (0.61 ms) was shorter than that of CdS/ITO electrode (0.95 ms), which was assigned to the fast charge transfer of CdS/MoS_2 heterojunction. Moreover, the τ_n derived from IMVS reflected the recombination process of photoelectrode (Fig. 3C). The average lifetime for CdS (curve a) and CdS/MoS_2 modified ITO electrode (curve b) were 115.4 ms and 408.3 ms, respectively. These results suggested the recombination process of electron–hole pairs was inhibited by the formed heterostructure, which is consistent with the IMPS results.

Fig. 3D displayed the typical photocurrent–time curves to further investigate the photoelectrochemical performance of heterojunction-based biosensor. The photocurrent intensity of HLDP:C-DNA/CdS/MoS_2 modified ITO electrode (curve b) was 2.8 times higher than that of HLDP:C-DNA/CdS modified electrode (curve a). The enhanced photocurrent effect of CdS/MoS_2 heterostructure in present work was better 2.3 times of dual-functional MoS_2 sheet-modified CdS branch (Min et al., 2014), which may attribute to the close integration of homogeneously dispersed CdS QDs and MoS_2 QDs in contact interface. Overall, the heterojunction-based biosensor could be utilized to detect DNA without external irradiation.

The electron transfer pathway of CdS/MoS_2/ITO electrode was illustrated to explain the possible mechanism of enhanced photoelectrochemical activity (Scheme 1). Under irradiation, the separation of electron–hole pairs could occur in CdS QDs, and the reformed band edge in CdS/MoS_2 heterojunction would cause the rapid transportation of photogenerated electrons from the VB of CdS QDs to that of MoS_2 QDs and then to ITO electrode. Meanwhile, the holes of MoS_2 QDs would migrate to the CB of CdS QDs, and can be sacrificed by the donor of H_2O_2. Obviously, such a synergy effect of CdS/MoS_2 hybrids could hasten the spatial charge separation of charge carriers along with enhanced electron transport rate, resulting in the significant improvement of photocurrent response.

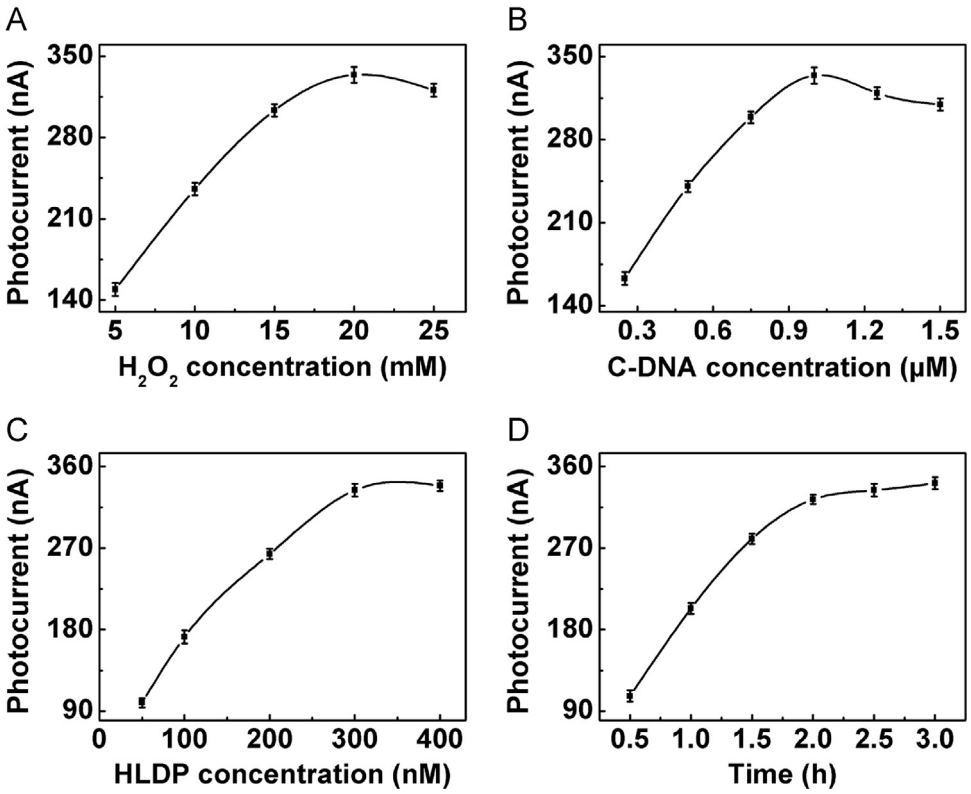

Fig. 4. Effects of (A) H_2O_2 concentration, (B) C-DNA concentration, (C) HLDP concentration, and (D) incubation time of CHA reaction on the photocurrent response of the biosensor.

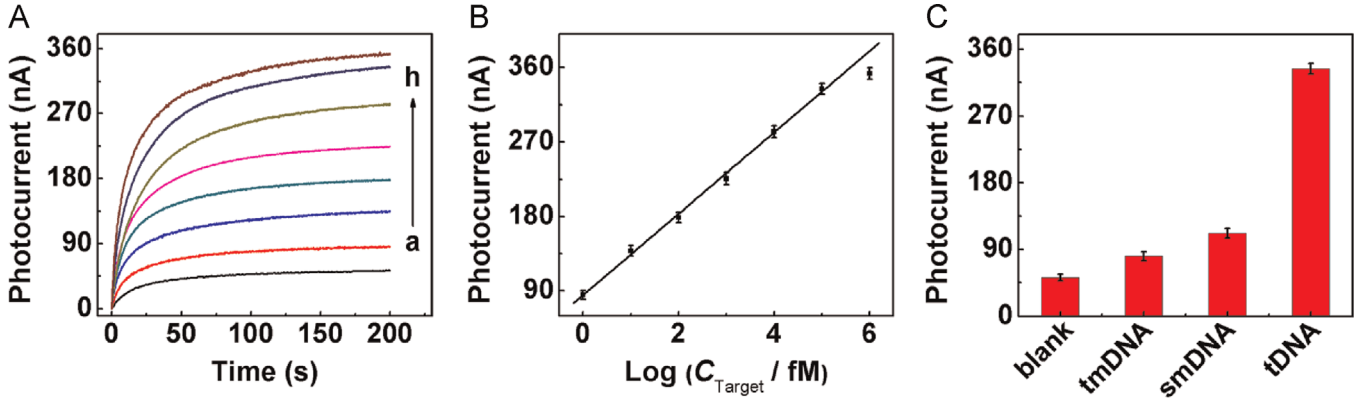

Fig. 5. (A) Photocurrent response of the proposed biosensor at 0, 1, 10, 100, 1000, 10,000, 100,000, and 1,000,000 fM target DNA (from a to h). (B) Calibration curve of photocurrent versus logarithm of target DNA concentration. (C) Photocurrent response of the designed biosensor to blank, 100 pM of tmDNA, smDNA and target DNA. The photocurrent intensities were recorded at 200 s.

3.4. Optimization of detection conditions

To achieve optimal photoelectrochemical response, several experimental parameters including H_2O_2 concentration, C-DNA concentration, HLDP concentration and incubation time of CHA were investigated (Fig. 4). Because H_2O_2 served as an electron donor for generation of photocurrent as well as a coreagent for chemiluminiscence, the concentration of H_2O_2 depended largely on the sensitive assay of DNA. The photocurrent was enhanced with the increasing of H_2O_2 concentration up to 20 mM and then slightly decreased with further addition of H_2O_2 (Fig. 4A), which was attributed to the surface oxidation of CdS QDs caused by excess H_2O_2 (Mancini et al., 2008). Thus, 20 mM H_2O_2 was selected for the next experiments. Similarly, when C-DNA concentration was increased, the photocurrent increased gradually in the range of 0.25–1.0 μM and in turn declined with the further increasing of C-DNA (Fig. 4B), indicating that high concentration of C-DNA could reduce the efficiency of DNA hybridization resulted from steric hindrance (Zhang et al., 2006). Therefore, 1.0 μM C-DNA was employed for the construction of biosensor.

To investigate the effect of the concentration of HLDP acting as CHA primer on biosensor performance, 0.1 nM target DNA was mixed with HLDP at different concentrations ranging from 0 to 400 nM. As shown in Fig. 4C, the photocurrent signal increased significantly and then tended to a plateau at 300 nM, suggesting the saturated binding of C-DNA to HLDP. Thus, 300 nM HLDP was selected for catalytic hairpin assembly. Moreover, the incubation time of CHA on modified electrode surface was also optimized (Fig. 4D). When the incubation time was more than 2.5 h, no obvious photocurrent change was observed, indicating CHA reaction

nearly reached the maximum. So, 2.5 h was chosen as the optimal reaction time.

In addition, the applied potential was also an important parameter for photocurrent generation. With the increasing potential from +0.1 to +0.3 V, a significant increase of photocurrent was obtained. Since the photocurrent at +0.2 V was 87% of that at +0.3 V, providing enough sensitivity for DNA detection. Thus, +0.2 V was chosen for next experiments.

3.5. Analytical performance

Under optimized conditions, the CdS/MoS_2 heterojunction-based biosensor could be conveniently used for DNA detection. As shown in Fig. 5A, with the increasing target DNA concentration, the photocurrent intensity increased gradually, indicating that the formed HLDP:C-DNA duplex could produce luminol chemiluminescence to facilitate the excitation of CdS QDs. The calibration plot of photocurrent intensity versus the logarithm of target DNA concentration from 1 fM to 100 pM showed a good linearity (Fig. 5B). The linear range was wider than that of photoelectrochemical biosensor by means of catalase mimetics of bio-barcoded platinum nanoparticles/hemin/G-quadruplex (0.2 pM–1 nM) (Wang et al., 2015), fluorescence biosensor via CHA-programmed Mg^{2+}-dependent DNAzyme (0.5 pM–20 nM) (Liu et al., 2015), and chemiluminescence biosensor based on exonuclease III-mediated cascade amplification (10 fM–1 pM) (Gao and Li, 2014). The regression equation was I (nA) = 85.10 + 49.09 log C (fM) with a correlation coefficient of 0.997, where I is the photocurrent of the biosensor and C is the concentration of target DNA. The detection limit was estimated to be 0.39 fM at 3σ, which was much lower than 9 fM of hybridization chain reaction-based photoelectrochemical amplification (Li et al., 2015), 92 fM of exonuclease III-assisted target recycling and CHA-based electrochemical method (Tao et al., 2015), and 81 fM of target-triggered quadratic amplification-based colorimetric methods (Wu et al., 2015). Apparently, the CdS/MoS_2 modified electrode with excellent photoelectricity activity is a promising sensing platform for DNA bioanalysis.

The selectivity of the designed biosensor was evaluated by the photocurrent toward blank and other DNA samples such as tDNA, smDNA and tmDNA (Fig. 5C). As expected, the photoelectrochemical measurements showed obvious photocurrent response to tDNA, which was 3.0-, 4.1- and 6.4-fold higher than that of smDNA, tmDNA and blank samples, respectively. These results indicated the proposed biosensor was highly selective for tDNA against base mismatched sequences owing to the specific biorecognition of DNA hybridization followed by CHA reaction.

4. Conclusions

This work was successfully constructed a highly efficient CdS/MoS_2 heterojunction-based photoelectrochemical sensing platform for ultrasensitive detection of DNA via CHA and dual hemin-induced chemiluminescence amplification. The formation of heterojunction through contact of two quantum dots could retard the recombination of electron–hole pairs, resulting in 280% enhancing of photocurrent. This observation was related to the fast transfer rate and the long lifetime of photogenerated carriers in CdS/MoS_2-based detection system. In the presence of target DNA, C-DNA could initiate CHA reaction to product HLDP:C-DNA as signal probe on electrode surface, leading to the significant enhancement of photocurrent under amplified chemiluminescence excitation. Considering the high photoconversion efficiency of CdS/MoS_2 heterojunction, the biosensor showed favorable performance with wide linear range, excellent sensitivity and desirable selectivity. The two semiconductor-based heterostructure provides a universal platform for the construction of photoelectrochemical devices in ultrasensitive bioanalysis.

Acknowledgments

We gratefully acknowledge the National Natural Science Foundation of China (21375060, 21135002, 21121091) and Priority development areas of National Research Foundation for the Doctoral Program of Higher Education of China (20130091130005).

References

Bai, S., Wang, L.M., Chen, X.Y., Du, J.T., Xiong, Y.J., 2015. Nano Res. 8, 175–183.
Chen, J.Z., Wu, X.J., Yin, L.S., Li, B., Hong, X., Fan, Z.X., Chen, B., Xue, C., Zhang, H., 2015. Angew. Chem. Int. Ed. 54, 1210–1214.
Chen, Y., Xu, J., Su, J., Xiang, Y., Yuan, R., Chai, Y.Q., 2012. Anal. Chem. 84, 7750–7755.
Chikan, V., Kelley, D.F., 2002. J. Phys. Chem. B 106, 3794–3804.
Choi, K., Raza, S.R.A., Lee, H.S., Jeon, P.J., Pezeshki, A., Min, S.W., Kim, J.S., Yoon, W., Ju, S.Y., Lee, K., Im, S., 2015. Nanoscale 7, 5617–5623.
Deng, S.Y., Cheng, L.X., Lei, J.P., Cheng, Y., Huang, Y., Ju, H.X., 2013. Nanoscale 5, 5435–5441.
Gao, W.Y., Wang, M.Q., Ran, C.X., Li, L., 2015. Chem. Commun. 51, 1709–1712.
Gao, Y., Li, B.X., 2014. Anal. Chem. 86, 8881–8887.
Garai-Ibabe, G., MÖller, M., Saa, L., Grinyte, R., Pavlov, V., 2014. Anal. Chem. 86, 10059–10064.
Gill, R., Zayats, M., Willner, I., 2008. Angew. Chem. Int. Ed. 47, 7602–7625.
Golub, E., Niazov, A., Freeman, R., Zatsepin, M., Willner, I., 2012. J. Phys. Chem. C 116, 13827–13834.
Gopalakrishnan, D., Damien, D., Shaijumon, M.M., 2014. ACS Nano 8, 5297–5303.
Gopalakrishnan, D., Damien, D., Li, B., Gullappalli, H., Pillai, V.K., Ajayan, P.M., Shaijumon, M.M., 2015. Chem. Commun. 51, 6293–6296.
Ha, H.D., Han, D.J., Choi, J.S., Park, M., Seo, T.S., 2014. Small 10, 3858–3862.
Haddache, F., Le Goff, A., Reuillard, B., Gorgy, K., Gondran, C., Spinelli, N., Defrancq, E., Cosnier, S., 2014. Chem. Eur. J. 20, 15555–15560.
Hun, X., Xie, G.L., Luo, X.L., 2015. Chem. Commun. 51, 7100–7103.
Kang, Y.M., Gong, Y.J., Hu, Z.J., Li, Z.W., Qiu, Z.W., Zhu, X., Ajayan, P.M., Fang, Z.Y., 2015. Nanoscale 7, 4482–4488.
Krüger, J., Plass, R., Grätzel, M., Cameron, P.J., Peter, L.M., 2003. J. Phys. Chem. B 107, 7536–7539.
Li, C.X., Wang, H.Y., Shen, J., Tang, B., 2015. Anal. Chem. 87, 4283–4291.
Li, J., Tu, W.W., Li, H.B., Han, M., Lan, Y.Q., Dai, Z.H., Bao, J.C., 2014. Anal. Chem. 86, 1306–1312.
Liu, S.F., Cheng, C.B., Gong, H.W., Wang, L., 2015. Chem. Commun. 51, 7364–7367.
Long, Y.T., Kong, C., Li, D.W., Li, Y., Chowdhury, S., Tian, H., 2011. Small 7, 1624–1628.
Lu, W., Wang, G., Jin, Y., Yao, X., Hu, J.Q., Li, J.H., 2006. Appl. Phys. Lett. 89, 263902.
Lu, W., Jin, Y., Wang, G., Chen, D., Li, J.H., 2008. Biosens. Bioelectron. 23, 1534–1539.
Mancini, M.C., Kairdolf, B.A., Smith, A.M., Nie, S.M., 2008. J. Am. Chem. Soc. 130, 10836–10837.
Min, Y.L., He, G.Q., Xu, Q.J., Chen, Y.C., 2014. J. Mater. Chem. A 2, 2578–2584.
Qian, Y., Tang, D.Q., Du, L.L., Zhang, Y.Z., Zhang, L.X., Gao, F.L., 2015. Biosens. Bioelectron. 64, 177–181.
Qing, Z.H., He, X.X., Huang, J., Wang, K.M., Zou, Z., Qing, T.P., Mao, Z.G., Shi, H., He, D.G., 2014. Anal. Chem. 86, 4934–4939.
Ou, J.Z., Chrimes, A.F., Wang, Y.C., Tang, S.Y., Strano, M.S., Kalantar-zadeh, K., 2014. Nano Lett. 14, 857–863.
Ren, X.P., Pang, L.Q., Zhang, Y.X., Ren, X.D., Fan, H.B., Liu, S.Z., 2015. J. Mater. Chem. A 3, 10693–10697.
Russell, C., Welch, K., Jarvius, J., Cai, Y.X., Brucas, R., Nikolajeff, F., Svedlindh, P., Nilsson, M., 2014. ACS Nano 8, 1147–1153.
Singh, A.K., Andleeb, S., Singh, J., Dung, H.T., Seo, Y., Eom, J., 2014. Adv. Funct. Mater. 24, 7125–7132.
Song, W.L., Zhang, Q., Sun, W.B., 2015. Chem. Commun. 51, 2392–2395.
Sun, W.T., Yu, Y., Pan, H.Y., Gao, X.F., Chen, Q., Peng, L.M., 2008. J. Am. Chem. Soc. 130, 1124–1125.
Tao, C.Y., Yan, Y.R., Xiang, H., Zhu, D., Cheng, W., Ju, H.X., Ding, S.J., 2015. Chem. Commun. 51, 4220–4222.
Wang, G.L., Liu, K.L., Shu, J.X., Gu, T.T., Wu, X.M., Dong, Y.M., Li, Z.J., 2015. Biosens. Bioelectron. 69, 106–112.
Wang, J., Mora-Seró, I., Pan, Z.X., Zhao, K., Zhang, H., Feng, Y.Y., Yang, G., Zhong, X.H., Bisquert, J., 2013. J. Am. Chem. Soc. 135, 15913–15922.
Wang, T.Y., Zhu, R.Z., Zhuo, J.Q., Zhu, Z.W., Shao, Y.H., Li, M.X., 2014. Anal. Chem. 86, 12064–12069.
Willner, I., Shlyahovsky, B., Zayats, M., Willner, B., 2008. Chem. Soc. Rev. 37, 1153–1165.
Wu, H., Liu, Y.L., Wang, H.Y., Wu, J., Zhu, F.F., Zou, P., 2015. Biosens. Bioelectron. 66, 277–282.
Wu, Y.P., Zhang, B.T., Guo, L.H., 2013. Anal. Chem. 85, 6908–6914.
Xiao, F.X., Miao, J.W., Liu, B., 2014. J. Am. Chem. Soc. 136, 1559–1569.

Xu, G.B., Dong, S.J., 1999. Electroanalysis 11, 1180–1184.
Zang, Y., Lei, J.P., Ling, P.H., Ju, H.X., 2015. Anal. Chem. 87, 5430–5436.
Zhang, J., Song, S.P., Zhang, L.Y., Wang, L.H., Wu, H.P., Pan, D., Fan, C.H., 2006. J. Am. Chem. Soc. 128, 8575–8580.
Zhang, K., Kim, W.J., Ma, M., Shi, X.J., Park, J.H., 2015. J. Mater. Chem. A 3, 4803–4810.
Zhang, X.R., Zhao, Y.Q., Zhou, H.R., Qu, B., 2011. Biosens. Bioelectron. 26, 2737–2741.
Zhang, X.R., Xu, Y.P., Yang, Y.Q., Jin, X., Ye, S.J., Zhang, S.S., Jiang, L.L., 2012. Chem. Eur. J. 18, 16411–16418.
Zhao, H., Dong, Y.M., Jiang, P.P., Miao, H.Y., Wang, G.L., Zhang, J.J., 2015. J. Mater. Chem. A 3, 7375–7381.
Zhao, W.W., Xu, J.J., Chen, H.Y., 2014. Chem. Rev. 114, 7421–7441.
Zhou, K.G., Mao, N.N., Wang, H.X., Peng, Y., Zhang, H.L., 2011. Angew. Chem. Int. Ed. 50, 10839–10842.
Zhou, W.J., Yin, Z.Y., Du, Y.P., Huang, X., Zeng, Z.Y., Fan, Z.X., Liu, H., Wang, J.Y., Zhang, H., 2013. Small 9, 140–147.
Zhuang, J.Y., Lai, W.Q., Xu, M.D., Zhou, Q., Tang, D.P., 2015. ACS Appl. Mater. Interfaces 7, 8330–8338.